LRRK2 Deficiency Impairs *trans*-Golgi to Lysosome Trafficking and Endocytic Cargo Degradation in Human Renal Proximal Tubule Epithelial Cells

Nathan J. Lanning[1], Calvin VanOpstall[2], Megan L. Goodall[1], Jeffrey P. MacKeigan[1], and Brendan D. Looyenga[1,2]

[1]Van Andel Research Institute, Lab of Systems Biology, 333 Bostwick Ave, Grand Rapids, MI 49509 USA
[2]Calvin College, Department of Chemistry & Biochemistry, 1726 Knollcrest Circle SE, Grand Rapids, MI 49546 USA

N.J.L. performed fluorescence microscopy and quantification associated with Figures 1-3.
C.VO. assisted with experimental design and execution in Figures 4 and 6.
M.L.G. performed electron microscopy associated with Figure 3.
J.P.M. assisted in conception and design of experiments.
B.D.L. conceived of projected, designed experiments and performed all experiments not specified below; primary and senior author of manuscript.
All authors discussed results and contributed review comments for the final manuscript.

Running head:

LRRK2 deficiency impairs vesicle trafficking in tubule cells

Address for Correspondence:

Brendan D. Looyenga, PhD
Assistant Professor
Department of Chemistry & Biochemistry
Calvin College
1726 Knollcrest Circle SE
Grand Rapids, MI 49546
blooye62@calvin.edu
616-526-8493

Abstract

Defects in vesicular trafficking underlie a wide variety of human diseases. Genetic disruption of leucine-rich repeat kinase 2 (LRRK2) in rodents results in epithelial vesicular trafficking errors that can also be induced by treatment of animals with LRRK2 kinase inhibitors. Here we demonstrate that defects in human renal cells lacking LRRK2 phenocopy those seen in the kidneys of *Lrrk2* knockout mice, characterized by accumulation of intracellular waste vesicles and fragmentation of the Golgi apparatus. This phenotype can be recapitulated by knockdown of N-ethylmaleimide sensitive factor (NSF), which physically associates with LRRK2 in renal cells. Deficiency in either protein leads to a defect in *trans*-Golgi to lysosome protein trafficking, which compromises the capacity of lysosomes to degrage endocytic and autophagic cargo. In contrast, neither bulk endocytosis nor autophagic flux are impaired when LRRK2 is acutely knocked down in HK2 cells. These data collectively suggest that the primary renal defect caused by LRRK2 deficiency is in protein trafficking between the Golgi apparatus and late endosome/lysosome, which leads to progressive impairments in lysosomal function.

Key words

LRRK2

NSF

vesicle trafficking

Golgi apparatus

lysosome

Introduction

Activating mutations to human *LRRK2* are now well-established drivers of Parkinson's Disease (PD)(30, 39). Because most—if not all—of these mutations increase the kinase activity of LRRK2, pharmacologic inhibition of this enzyme has been an attractive target for PD therapy(16, 34). Two limiting factors for such drugs are their ability to penetrate the brain and the potential for dose-limiting side effects on peripheral tissues. Though the former limitation has largely been overcome, animal studies with brain penetrant LRRK2 inhibitors have demonstrated that chronic inhibition of LRRK2 is associated with toxicity to the pulmonary epithelia(10, 14, 18). This toxicity is phenotypically similar to defects seen in *Lrrk2* knockout mice, suggesting a role of LRRK2 in normal Type II pneumocyte function(14, 38). Perhaps surprising, however, is the relative lack of toxicity in the kidneys of drug-treated animals given that both *Lrrk2* knockout mice and rats display profound renal dysfunction associated with cellular defects in vesicular trafficking and lysosomal function(4, 38). Whether this points to distinct enzymatic roles for LRRK2 in pulmonary and renal epithelia or a lack of cellular exposure to LRRK2 inhibitors in the kidney is unclear.

The effect of LRRK2 kinase inhibition in the kidney is also of significance based on studies that demonstrate *LRRK2* is chromosomally amplified and overexpressed in papillary renal cell carcinoma (pRCC)(2, 23). Perturbation of LRRK2 expression in human pRCC cell lines results in cell cycle arrest and selective inhibition of key cell signaling pathways, most likely via the disruption of signal transduction by growth factor receptors. Other studies have uncovered LRRK2 overexpression or mutation in a variety of solid tumors, as well as epidemiological evidence that PD-associated mutations to LRRK2 (G2019S) increase the risk of several non-skin cancers(1, 20, 33). Together these data suggest that LRRK2 kinase inhibitors may potentially be repurposed for cancer therapy, providing they can be used for a relatively short period of time to avoid peripheral toxicity to the lung. Understanding the molecular role of LRRK2 in cancer and normal tissues is therefore of paramount importance.

Most current literature supports a role for LRRK2 in vesicular trafficking processes downstream of endocytosis, such as autophagy and cargo sorting(3, 24, 26, 35). Precisely where in these processes LRRK2 is involved is less clear, as it appears to physically interact with and/or phosphorylate a number of protein substrates known to be involved in vesicular trafficking. Most prominent among these substrates are Rab family GTPases, particularly those involved in late endosomal sorting(6, 15, 24, 36). Given that the renal and pulmonary phenotypes of *Lrrk2*-

/- mice include the epithelial accumulation of intracellular vesicles containing undigested waste, it seems probable that LRRK2 regulates late endosomal compartment homeostasis via its interactions with Rab family GTPases and other vesicular trafficking proteins (19, 38). The central role of this compartment in endocytic cargo sorting may also explain the propensity for amplification or mutation of *LRRK2* across several solid tumor types, as it is now well established that alterations to endosomal trafficking machinery play an important role in cancer development(12).

In addition to its interactions with Rab proteins, LRRK2 has also been shown to interact with N-ethylmaleimide sensitive fusion (NSF) protein, which functions as an ATP-dependent disassembly factor for *cis*-SNARE complexes after vesicular fusion(7, 31). Though this activity of NSF is its most prominent function—and the one implicated in its interaction with LRRK2—it has also been shown to mediate restacking of Golgi apparatus fragments into discreet cisternae after the completion of mitosis, which is necessary for proper vesicular trafficking between the Golgi apparatus and other cellular compartments(5, 32). Unlike its SNARE disassembly function, this secondary role for NSF is independent of its ATPase activity though it appears to be conserved in metazoans as simple as *Drosophila*(28). Whether interactions between LRRK2 and NSF also impact Golgi integrity and sorting between the Golgi and other compartments is unknown. In this study we address this issue in the context of human renal epithelial cells and present findings that suggest the vesicular trafficking defects previously identified in LRRK2-deficient cells are centrally related to disorganization of the Golgi apparatus.

Materials and Methods

Antibodies and Reagents

Rabbit monoclonal or polyclonal antibodies for Rab5, Rab7, NSF, LC3B and STX6 used for immunoblotting and immunofluorescent staining were purchased from Cell Signaling Technology (CST, Danver, MA). The anti-LRRK2 (UDD3), anti-LRRK2 (MJFF2) anti-phospho-LRRK2-S935, anti-GBA and anti-ARSB rabbit monoclonal antibodies were obtained from Epitomics (Epitomics/Abcam, Cambridge, MA). The anti-β-actin and tubulin mouse monoclonal antibodies used for immunoblotting were obtained from Sigma-Aldrich (Sigma, St. Louis, MO). The anti-V5 epitope mouse monoclonal antibody and AlexaFluor-conjugated goat secondary antibodies were obtained from Invitrogen/Life Technologies (Thermo-Fisher Scientific, Grand Island, NY). The anti-p62/SQSTM1, EEA1, LAMP1 and gm130 mouse monoclonal antibodies

used for immunofluorescent staining were obtained from Becton Dickinson (BD Biosciences, San Jose, CA). All antibodies were used at the dilutions recommended by each manufacturer unless otherwise specified.

All chemical reagents were obtained from Sigma-Aldrich unless otherwise indicated. The LRRK2 catalytic inhibitor GNE-7915 was purchased from Selleck Chemicals (Houston, TX) and used at the indicated concentrations. The LRRK2 inhibitor PFE-475 (PFE-06447475) was provided by Dr. Jaclyn Henderson (Pfizer, New York, NY). Vesicular trafficking cargoes AlexaFluor488-transferrin, AlexaFluor488-dextran and BZiPAR (Rhodamine 110, bis-(CBZ-L-Isoleucyl-L-Prolyl-L-Arginine Amide), Dihydrochloride) were purchased from Invitrogen/Life Technologies and used at the indicated concentrations.

Immunohistochemistry

Murine renal tissues were obtained as a gift from Dr. Ted Dawson (Johns Hopkins University, Baltimore, MD). The tissues were harvested from necropsied *Lrrk2-/-* animals and wild-type littermates in compliance with approved animal care guidelines from Johns Hopkins Committee Institutional Animal Care and Use Committee. Tissues were fixed for ~24 hours in 4% paraformaldehyde, washed with cold phosphate buffered saline (PBS) and stored at 4°C in 70% ethanol. The tissues were then dehydrated through graded ethanols and methyl salicylate, and then embedded in paraffin prior to sectioning. Kidney sections were cut at 5 micron thickness and floated onto glass slides for drying at 37°C to promote adherence. After drying, sections were deparaffinized, rehydrated and stained with hematoxylin and eosin using a Symphony Automated H&E stainer (Ventana Medical Systems, Tucson, AZ) in the Van Andel Institute Core Facility. Images were captured with an ECLIPSE Ci photomicroscope (Nikon Instruments, Melville, NY) at 20x and 40x resolution.

Cell Culture

Normal immortalized human kidney (HK2) cells were purchased from American Type Culture Collection (ATCC, Manassas, VA) and maintained in RPMI-1640 media supplemented with 2 mM GlutaMAX (Thermo-Fisher Scientific, Grand Island, NY) and 10% fetal bovine serum (FBS). HEK-293FT cells were obtained from Invitrogen/Life Technologies (Thermo-Fisher Scientific) and maintained in standard DMEM with high glucose (4.5 g/L) and 10% FBS. Both cell lines were incubated in a humidified and sterile tissue culture incubator at 37°C with 5% CO_2 atmosphere. Stable HK2 polyclonal cell lines expressing short hairpin RNAs (shRNAs) were

162 produced by infecting cells with conditioned viral media from 293FT producer cells that had
163 been diluted 1:10 in HK2 media and supplemented with 8.0 µg/mL polybrene. After 48-72 hours
164 incubation, cells were replated in culture media containing 2 µg/mL puromycin to select for cells
165 with integrated lentivirus. Because long-term depletion of LRRK2 and NSF (>2 weeks) results
166 in increased HK2 cell death, all assays that utilized stable shRNA lines were performed on
167 freshly selected cells without further passaging or freeze/thaw cycles.
168
169 Amino acid starvation of cells was performed by washing them with Dulbeccos' Phosphate
170 Buffered Saline (DPBS) and refeeding with DPBS supplemented with 20 mM HEPES buffer (pH
171 7.2), insulin-transferrin-selenium (ITS, Thermo-Fisher Scientific), 10 mM D-glucose and 1x
172 RPMI vitamins (Sigma-Aldrich) lacking all amino acids. To block autophagosome processing by
173 lysosomal acidification, cells were treated in parallel with bafilomycin A1 (50 nM) along with
174 amino acid starvation.
175
176 *Lentiviral Vector Production*
177 Validated lentiviral shRNA vector plasmids from The RNA Consortium (TRC) pLKO.1 collection
178 were obtained from Sigma-Aldrich (Sigma). Each lentiviral plasmid was transfected into a 10
179 cm dish containing 1.5 million 293FT cells along with ViraPower third generation packaging
180 plasmids (pLP1, pLP2 and pVSVG; Thermo-Fisher Scientific) using standard calcium phosphate
181 precipitation. Media was changed the following day and allowed to incubate on cells for 72
182 hours prior to harvest. The 10 mL of conditioned media from each lentiviral vector was removed
183 and filtered through a 0.4 micron syringe filter before freezing at -80°C in 1 mL aliquots.
184
185 *Immunofluorescence microscopy*
186 Parental HK2 cells or stable polyclonal cell lines expressing shRNAs were seeded to glass
187 coverslips or glass bottom 96-well plates (Greiner Bio-One, Monroe, NC) in culture media and
188 allowed to adhere overnight under standard tissue culture conditions. Treatment of cells prior to
189 fixation and staining is indicated in each data Fig.. Cells were fixed with 3.7% formaldehyde in
190 PBS solution and permeabilized with 0.2% Triton X-100 on ice. After blocking in 5% normal
191 goat serum (Sigma) in PBS solution, the cells were incubated with the indicated primary
192 antibody diluted in blocking buffer overnight at 4°C. The following day cells were washed with
193 PBS containing 0.05% Tween-20 (PBS-T) and stained with AlexaFluor-488 coupled goat anti-
194 rabbit and AlexaFluor-546 coupled goat anti-mouse secondary antibodies (Invitrogen/Life
195 Technologies) diluted at 1:1,000 in blocking buffer for 1 hour at room temperature. After a

second round of washing in PBS-T, the cells were nuclear counter-stained with DAPI (1 µg/mL) and prepared with gel mounting media prior to mounting on glass slides. Epifluorescent images of cells were obtained using a Nikon Ti-E inverted fluorescence microscope equipped with DAPI, FITC, and Texas Red filter sets and processed using the NIS Elements software package (Nikon Instruments). Confocal images were obtained using a Nikon A1plus-RSi scanning confocal microscope equipped with 403, 488, 561 and 640 nm solid-state lasers and a 32-detector spectral imager (Nikon Instruments). All images were processed and quantified using the NIS Elements software package (Nikon Instruments).

Immunoblotting

Cells cultured in 6-well dishes were rinsed with cold PBS and harvested into 100 µL of lysis buffer (20 mM Tris [pH 7.5], 150 mM NaCl, 1 mM EDTA, 1 mM EGTA, 2.5 mM sodium pyrophosphate, 1 mM sodium glycerophosphate, 1 mM sodium orthovanadate, 0.5% NP40, 0.1% Brij35, 0.1% sodium deoxycholate) supplemented with mammalian cell protease inhibitor cocktail (Sigma-Aldrich). Each lysate was homogenized by brief sonication at 30% power on ice and then cleared by centrifugation at 10,000 relative centrifugal forces (rcf) for 5 min at 4°C. Concentration of each lysate was determined by Bradford assay along with a two-fold serial dilution of 10 mg/mL BSA to generate a standard curve. Equal amounts of protein lysate (20-50 µg) were separated by reducing polyacrylamide gel electrophoresis and transferred overnight to nitrocellulose membrane using a traditional wet transfer apparatus (TE62 model; Hoefer, Holliston, MA). The blots were blocked with 3% non-fat dry milk in Tris-buffered saline containing 0.05% Tween-20 (TBST), and then probed overnight at 4°C with primary antibodies diluted to the manufacturer's specification. After washing off unbound primary antibody, the membranes were incubated for 1 hour at room temperature with goat anti-rabbit-IRDyeTM800 and goat anti-mouse-IRDyeTM680 secondary antibodies (LiCor, Lincoln, NE), and then imaged with an Odessey scanner (LiCor). Images were processed with the Odyssey Infrared ImaginingSystem software (version 3.0.25) to ensure that signal was in the linear range of photon detection prior to export in TIFF format.

Immunoprecipitation

Cells cultured in 10 cm dishes were rinsed with cold PBS and harvested into 0.4 mL of immunoprecipitation buffer (50 mM HEPES [pH 7.0], 150 mM NaCl, 1 mM EDTA, 1 mM EGTA, 5 mM sodium pyrophosphate, 10 mM sodium glycerophosphate, 50 mM sodium fluoride, 1 mM sodium orthovanadate, 0.1% NP40, 10% glycerol) supplemented with mammalian cell protease

inhibitor cocktail and N-ethylmaleimide when indicated (Sigma-Aldrich). The lysates were homogenized by shearing through a 25-gauge needle on ice and cleared by centrifugation at 10,000 rcf for 5 min at 4°C. Lysates were quantified by Bradford assay as above, and equal protein amounts (0.5-1 mg) were incubated for 1 hour at 4°C with anti-LRRK2-UDD3 antibody (Abcam) diluted 1:100 in a final volume of 1 mL. Affinity complexes were precipitated by addition of 50 µL of equilibrated protein-G agarose beads (Invitrogen/Life Technologies) and incubation at 4°C with rotation for an additional hour. Bead pellets were washed three times with 0.9 mL volumes of buffer and eluted by boiling in 80 µL of 2x Laemmli Buffer (120 mM Tris [pH 6.8], 4% SDS, 20% glycerol, 0.02% bromophenol blue, 50 mM DTT).

Transmission Electron Microscopy

HK2 stable cell lines grown in 10 cm dishes were trypsinized, pelleted, washed in PBS and resuspended in 2% glutaraldehyde for fixation (Sigma). The cell pellets were then embedded in 2% agarose, postfixed in osmium tetroxide, and dehydrated with graded acetones. Samples were embedded in Poly/Bed 812 resin and polymerized at 60°C for 24 hours. Ultrathin sections (70 nm) were generated with a Power Tome XL (Boeckeler Instruments, Tucson, Arizona) and placed on copper grids. Cells were examined using a JEOL 100C× Transmission Electron Microscope at 100 kV (Tokyo, Japan). Electron microscopy services were performed by the Michigan State University Center for Advanced Microscopy (East Lansing, MI).

EdU Cell Proliferation Assay

Identification of proliferating cells found in the S-phase of the cell cycle was performed using the Click-iT EdU AlxaFluor488 imaging kit from Invitrogen/Life Technologies. In this assay the thymidine analog 5-ethynyl-deoxyuridine (EdU) was pulsed to cells at 10 µM for 1 hour under normal cell culture conditions, after which time the cells were fixed and stained for EdU incorporation using copper(I) catalyzed click chemistry. This assay covalently couples AlexaFluor488 to EdU, thereby labeling the nuclei of cells that were actively undergoing DNA replication during the 1 hour pulse. The mild conditions of this assay retain cellular protein stability and allow for subsequent immunofluorescent staining by standard methods.

Vesicular Trafficking Assays

Stable polyclonal HK2 cell lines expressing shRNAs were plated to 96-well plates at a density of 10,000 cells per well in RPMI-1640 media with 1% FBS and allowed to adhere overnight. The following day cells were starved of serum in basal RPMI-1640 media for 1 hour, and then

incubated with individual substrates for the indicated times prior to washing with PBS and fixation with 3.7% formaldehyde in PBS solution. AlexaFluor488-dextran was used at 10 μg/mL to monitor bulk phase endocytosis, while AlexaFluor488-transferrin was used at 50 μg/mL to monitor receptor-mediated endocytosis dependent on receptor recycling. At the end of the assay, 96-well plates were assayed at Ex/Em:488/510 nm in a Synergy H1 multimode plate reader (BioTek, Winooski, VT). For lysosomal trafficking assays, the fluorogenic peptide substrate BZiPAR was incubated with live cells at 50 μM concentration +/- 30 μM dynasore as a negative control for endocytic uptake. These assays were monitored continuously at Ex/Em:495/520 nm for 30 minutes in the Synergy H1 multimode plate reader warmed to 37°C with 5% CO_2 atmosphere. Fluorescent values from each substrate were normalized to cell number in each well using the CyQuant-NT nuclear dye (Invitrogen/Life Technologies) as a relative benchmark for cellular abundance. Assays were performed in triplicate, and graphed with standard deviations from each assay using the Prism software package (Mac version 6, GraphPad Software, La Jolla, CA). Data were best fit to standard linear or hyberbolic curves and analyzed for significance using student's T-test as indicated.

Cellular Fractionation

Isolation of distinct organelle populations from stable polyclonal HK2 cell lines was performed according the fractionation assay described by Mazzulli, *et al(25)*. Briefly, cells were plated to 15 cm dishes at a density of 8 million cells per plate and allowed to adhere overnight in RPMI-1640 media containing 10% FBS. The following day cells were washed on ice with cold PBS and scraped into 1 mL of fractionation buffer (10 mM HEPES [pH 7.4], 1 mM EDTA, 0.25 M sucrose) supplemented with mammalian cell protease inhibitor cocktail (Sigma). The cells were dounce homogenized on ice with 100 strokes, and the subsequent lysate was centrifuged at 6,800 rcf for 5 minutes at 4°C to pellet out the nuclear fraction and intact cells (P1). Supernatant from this fraction was removed and centrifuged at 17,000 rcf for 10 minutes at 4°C to isolate the lysosomal fraction (P2). Supernatant from the second centrifugation was again removed and spun a final time at 104,000 rcf in an ultracentrifuge for 1 hour at 4°C to isolate the microsomal fraction containing ER and golgi-derived vesicles (P3). Both the P2 and P3 fractions were washed once with fractionation buffer, and then resuspended in 0.1 mL of organelle lysis buffer (20 mM HEPES [pH 7.4], 150 mM sodium chloride, 1 mM EDTA, 1.5 mM magnesium chloride, 50 mM sodium fluoride, 2 mM sodium orthovanadate, 1% Triton X-100, 10% glycerol) to disrupt organelle membranes. Protein concentration from each fraction was determined by Bradford assay as above.

N-acetylglucosaminidase Activity Assay

The N-acetylglucosaminidase (NAG) activity found in lysosomes and microsomes was assessed using 4-methylumbelliferyl-N-acetyl-β-D-glucosaminide (MNDG) as a substrate. Cleavage of the glycosidic bond in this substrate by lysosomal hexosaminidases releases 4-methylubelliferone, which can be quantified by fluorescence plate reader. Assays were performed on 0.50 µg of total protein from each fraction, which was diluted in a final volume of 50 µL in 250 mM citrate buffer (pH 4.6) containing a saturating concentration of 1 mM MNDG. Fluorescence values at Ex/Em:355/460 nm were measured on a Synergy H1 plate reader (BioTek) at 1 minute intervals over a 15 minute assay, and then converted to product concentrations using a standard curve of known 4-methylubelliferone concentration. The slope of the linear plot from each assay was used to determine NAG activity values in nmol/min/µg of lysate. Each assay was performed three times in triplicate to determine average activity values and the standard deviation of activity in each fraction.

Quantitative RT-PCR

Total RNA was isolated from cells using a RNeasy kit (Qiagen) and then reversed transcribed to produce cDNA libraries with an iScript Select kit (BioRad), both of which were utilized according to the manufacturers' suggested protocols. Three separate biological replicates of cells in each condition were analyzed by quantitative PCR (qRT-PCR) using intron-spanning primers targeted to the mRNAs for *NSF* and the ribosomal housekeeping gene *RPL13A*. Sequences for these primers are as follows:

NSF-fwd: GGCTTACTGGTGAAGGACATT

NSF-rev: TTCCAACAACCAGTCCTACTTC

RPL13A-fwd: TAAACAGGTACTGCTGGGCCGGAA

RPL13A-rev: AAGGGTTGGTGTTCATCCGCTT

The RT-PCR was carried out in a ABI 7500 thermocycler using 2x SYBR Green mix with ROX reference dye (BioRad). The C_t values for each gene were determined by selecting the threshold of SYBR Green fluorescence at half intensity of the logarithmic phase of amplification. The ratio of *NSF/RPL13A* mRNA abundance was then determined for each sample to normalize relative gene expression, and the level of expression for control cells (HK2 with non-targeting shRNA) was set to 100%. Expression of *NSF* mRNA in cells with NSF or LRRK2 knockdown were compared relative to this standard.

Statistical analysis

Each experiment with triplicate samples was repeated a minimum of three times to ensure that results could be replicated. Data reporting enzymatic rates was analyzed with GraphPad Prism 6 software for line fitting, with statistical significance determined by a two-tailed t-test. Statistical significance is reported at $P < 0.05$ or $P < 0.01$ as indicated in Fig. legends.

Results

Depletion of LRRK2 in Human Renal Epithelial Cells Promotes Vesicular Accumulation

Consistent with several prior studies, we found that histological staining of renal tissue from *Lrrk2-/-* mice at 3 months of age reveals the accumulation of optically clear vesicular inclusions within the cytoplasm of cortical tubule epithelia (Fig. 1A). These inclusions are most prominent in the proximal tubule cells, which can be identified by their intraluminal brush border that is absent in distal tubule cells. To determine whether human cells derived from renal proximal tubule epithelia display similar defects in the absence of LRRK2, we stably infected an immortalized human cell line derived from this tissue with a lentiviral vector (pLKO.1) that expresses a previously validated shRNA targeted to the *LRRK2* mRNA(23). As a control HK2 cells were also transduced with a non-targeting shRNA (NT-sh) that lacks homology to the human coding genome. Simple phase-contrast microscopy of these cells demonstrates a notable increase in the percent of cells bearing large vesicular inclusions, many of which have prominent vacuole-like structures (Fig. 1B).

Given the wide range of vesicular trafficking phenomenon that have been associated with LRRK2 function in various cellular and whole animal models, we sought to determine the identity of the large vacuole-like structures that were frequently observed in the LRRK2-knockdown line of HK2 cells. We used immunofluorescent staining with a variety of specific antibodies that mark specific vesicular populations or organelles in the mammalian cell as indicated in Fig. 1C. We particularly focused on markers that elucidate the autophagic, endo-lysosomal and recycling pathways for vesicular trafficking, all of which have been related to defects in LRRK2 activity.

Immunofluorescent imaging of LRRK2-deficient and control cells showed no obvious defects in the early endosome (Fig. 1D) or autophagic pathways (Fig. 1E), though significant differences in

localization of late endosome/lysosomal (Fig. 1F) and Golgi markers (Fig. 1G) were apparent. Specifically, we found that roughly 70% of cells contained large, perinuclear vacuole-like inclusions uniformly stained positive for the late endosome marker Rab7, and that these inclusions were typically situated in the perinuclear region of cells next to LAMP1-positive lysosomes (Fig. 1F,H). These observations are consistent with a role for LRRK2 in vesicular sorting in renal epithelia, most likely in a post-endocytic compartment associated with cargo trafficking from the Rab7-positive late endosome to the lysosome.

Depletion of LRRK2 in Human Renal Epithelial Cells Causes Golgi Fragmentation

In addition to the vesicular accumulation phenotype noted above, immunofluorescent staining of LRRK2-deficient cells also revealed widespread Golgi fragmentation (Fig. 1G). Markers for distinct compartments of the Golgi—STX6 and GM130—were distributed over a larger area of the cell with an average size of nearly 2.5 times that found in control cells (Fig. 1I). While this expansion and fragmentation of the Golgi apparatus was apparent in all LRRK2-deficient cells, it was especially prominent in those that also displayed an enlarged Rab7-positive endosomal compartment (Fig. 1J). In contrast, the relatively small percentage of control cells that contained an enlarged Rab7-positive endosomal compartment showed no difference in average Golgi area compared to those with typical Rab7 staining (Fig. 1J).

To determine whether the expansion of the Golgi compartment was more specifically related to a loss of LRRK2 kinase activity, we treated cells with two selective LRRK2 kinase inhibitors—GNE-7915 and PFE-475—prior to imaging of the Golgi apparatus by immunofluorescent microscopy. Immunoblot analysis of total protein levels and the autophosphorylation site at S935 demonstrate that both drugs confer kinase inhibition up to 24 hours with little impact on protein stability (Fig 2A,B). Cells treated for 24 hours with each drug were subsequently imaged after staining cells with the Golgi markers STX6 and GM130 (Fig. 2C). In contrast to the effect of complete LRRK2 knockdown with shRNA, we observed few cells with complete Golgi fragmentation when LRRK2 kinase activity was pharmacologically blocked. We did, however, observe a milder expansion of the Golgi apparatus, which was still significantly enlarged compared to vehicle (DMSO) treated cells (Fig. 2D). These data suggest that the Golgi expansion phenotype observed after stable genetic depletion of LRRK2 is at least in part a result of its kinase activity being absent in HK2 cells, but that absence of protein—or a longer timeframe—may be required to elicit complete Golgi fragmentation.

Genetic Depletion of NSF Phenotypically Mimics LRRK2 Knockdown

Prior studies of LRRK2 function in neuronal vesicular trafficking identified the protein NSF as an interaction partner and target of LRRK2 kinase activity(7, 31). This finding is intriguing since NSF has been previously shown to play a key role in the disassembly and reassembly of Golgi stacks during and after mitosis, respectively(28, 32). The former role depends upon its ATPase activity, while the latter occurs independent of its known enzymatic function. Cellular depletion of NSF in epithelial cells promotes Golgi fragmentation and defects in receptor recycling, though it has little effect on cell viability or endocytosis(11). Given the defects seen in LRRK2-deficient HK2 cells, these data suggested a functional link between NSF and LRRK2 in renal epithelia.

To test this hypothesis, we stably infected HK2 cells with an shRNA that targets NSF and compared the phenotype of these cells with LRRK2 knockdown (Fig. 3). Immunofluorescent staining for the early and late endosomal compartments in these cells demonstrates the presence of Rab7-positive vesicular inclusions that are phenotypically similar to those seen after stable LRRK2 knockdown (Fig. 3A). Further characterization of the two knockdown lines by transmission electron microscopy revealed an increase in the number and size of electron-dense vesicular structures, which are characteristic of late endosomes and lysosomes, compared to control cells (Fig. 3B). The contents of these vesicles include whole organelles, membrane whorls, and electron-dense aggregates, suggesting that these represent endocytosed or autophagic material that is destined for lysosomal degradation, but has failed to be properly digested (Fig.3 C,D).

LRRK2 and NSF Physically and Functionally Interact in Renal Epithelial Cells

The similarity in phenotypes between cells lacking either LRRK2 or NSF prompted us to investigate whether the two proteins co-localize to the same compartment in HK2 cells using confocal microscopy. Because endogenous LRRK2 is found at very low levels in cultured HK2 cells, we expressed exogenous FLAG-LRRK2 under control of the human EF1a promoter to facilitate immunofluorescent detection (Fig. 4A). As a positive control, we first stained cells for total LRRK2 versus the FLAG epitope to show that signals overlapped in the expected pattern (Fig. 4B). After confirming a strong overlap correlation between these signals, we then stained and imaged cells for the FLAG epitope versus endogenous NSF, which also demonstrated statistically significant overlap by confocal microscopy (Fig. 4A,B). It is notable that NSF was detected on all vesicles that stain positive for LRRK2, though a sizable portion of NSF-positive vesicles do not appear to contain LRRK2 (Fig. 4A, inset). This observation suggests that NSF

is likely to play a broader role in vesicular trafficking events than LRRK2, which appears to be more restricted in its subcellular localization.

The relevance of LRRK2-NSF colocalization in cells is reinforced by results of co-immunoprecipitation experiments that demonstrate that NSF can be precipitated with endogenous LRRK2 in HK2 cells (Fig. 4C). The interaction between these two proteins is enhanced by addition of the NSF inhibitor N-ethylmaleimide (NEM) to cell lysis buffer, which effectively locks NSF into its homohexameric, ATP-bound state by inhibiting ATPase activity(8, 27). These findings demonstrate that LRRK2 and NSF physically interact in renal epithelia and suggest that these two proteins are functionally related to each other in the process of vesicular trafficking in the endo-lysosomal system.

A potential insight into how LRRK and NSF interact became apparent from monitoring levels of endogenous NSF in HK2 cells that stably expressed an shRNA targeted to LRRK2. We observed that stable knockdown of LRRK2 leads to a roughly 40% decrease in NSF at both the mRNA and protein levels (Fig. 4D,E). Precisely why endogenous NSF expression at the mRNA level would be decreased by LRRK2 depletion is unclear, though we suggest it is an indirect relationship because overexpressing LRRK2 at a variety of levels using a pseudotyped baculovirus system (BacMam) fails to increase NSF levels (Fig. 4F). Furthermore, exogenous re-expression of V5-tagged human NSF in cells with LRRK2 deficiency fails to rescue the Golgi expansion defect seen when LRRk2 is depleted (Fig. 4E, data not shown). Together these data support the possibility of a functional link between LRRK2 and NSF but exclude a mechanism in which LRRK2 simply regulates NSF protein levels in the renal epithelia.

Golgi Fragmentation after NSF or LRRK2 Depletion Occurs Independent of Cell Division

Because prior studies from our lab showed a decrease in cellular proliferation rate when LRRK2 is stably depleted from renal cancer cells, we asked the question of whether the effect of LRRK2 knockdown on Golgi structure in normal HK2 cells is simply an artifact of mitotic arrest(23). To answer this question, we performed pulse-chase labeling of cells with the thymidine analog 5-ethynyl-2-deoxyuridine (EdU), and subsequently fixed and stained them for incorporation of this marker using fluorescent click chemistry along with immunofluorescent staining for the Golgi marker GM130 (Fig. 5A). EdU incorporation provides a good proxy for S-phase entry in cells, which showed little difference when either LRRK2 or NSF was knocked down in HK2 cells (Fig. 5B). Importantly, EdU incorporation had no impact on Golgi size in control cells, though

depletion of either LRRK2 or NSF again caused an expansion in the gm130-positive Golgi compartment (Fig. 5C).

To evaluate whether the effect of LRRK2 and NSF on Golgi fragmentation occurred concomitant with cell cycle progression, we performed two experiments. In the first experiment, we pulse-labeled cells with EdU for 2 hours and then immediately fixed and stained them for GM130. In this context, control cells with EdU incorporation showed a small—but insignificant—increase in Golgi size, whereas LRRK2 and NSF depleted cells showed no difference, though their overall Golgi area was still significantly larger than that of control cells (Fig. 5D). These data show that while in S-phase—before mitotic Golgi fragmentation has occurred—cells lacking LRRK2 or NSF already have expanded Golgi compartments.

In the second experiment, we performed EdU pulse labeling as before, but followed that with a 6 hour media chase to allow for cells to progress through S-phase and into mitosis. Here we observed a significant expansion of the Golgi area in EdU-positive cells, consistent with a mitosis-associated fragmentation of the Golgi (Fig. 5E). Importantly, however, we also found that EdU-negative cells from the LRRK2 and NSF depleted lines still displayed significantly expanded Golgi compartments, indicating that loss of these two proteins leads to a loss of Golgi compaction independent of progression through S-phase and into mitosis.

Depletion of LRRK2 and NSF Impairs Trafficking of Endocytic Cargo

A previous study of HeLa cells after knockdown of NSF suggested that while endocytosis itself was unimpaired, the ability of cells to recycle endocytosed receptors back to the cell surface was blocked by the absence of NSF(11). We recapitulated these findings in HK2 cells using fluorescently labeled dextran as a marker for fluid phase bulk endocytosis and labeled transferrin as a marker for receptor-mediated endocytosis. After knockdown of LRRK2 or NSF, we observed no change in the rate of dextran uptake relative to control cells, which is consistent with the absence of a general endocytic defect (Fig. 6A,B). In contrast, the rate of transferrin uptake was significantly decreased when either of these proteins was depleted from HK2 cells (Fig. 6C). Because the continuous uptake of transferrin by its receptor (TfR) requires post-endocytic recycling, this finding suggests that both LRRK2 and NSF are required to maintain the recycling pathway after internalization of membrane cargo from the cell surface.

We next asked whether the late endosomal defect we first observed in HK2 cells lacking LRRK2 could be a result of improper sorting of endocytic cargo to the lysosomal compartment. In this context we used syntaxin-7 (STX7) as a positive control since this protein is required for proper transport of late endosomal proteins to the lysosome(29). As expected, knockdown of STX7 had no impact on uptake of dextran or transferrin, though it significantly decreased trafficking of a fluorogenic peptide substrate (BZiPAR) to the lysosomal compartment (Fig. 6A-D). A similar decrease in trafficking of this peptide was elicited by pre-treatment of cells with the inhibitor dynasore (30 μM), which prevents dynamin-mediated scission of endocytic vesicles (Fig. 6D). Interestingly, we found that LRRK2 depletion resulted in a roughly 25% increase in peptide trafficking rate to the lysosome, while depletion of NSF had no effect. This finding suggests that the waste accumulation defect seen in *Lrrk2-/-* mouse kidneys and in HK2 cells after LRRK2 knockdown may not be a result of decreased lysosomal trafficking per se, but rather a loss of lytic activity toward specific lysosomal substrates.

Depletion of LRRK2 and NSF Impairs Trafficking of Lysosomal Hydrolases

The finding that post-endocytic lysosomal sorting was normal—if not accelerated—in LRRK2 deficient cells prompted us to examine whether the two central vesicular trafficking defects seen upon LRRK2 or NSF depletion—expansion of the late endosome and fragmentation of the Golgi apparatus—are functionally related by a defect in *trans*-Golgi to late endosome transport. Among the various cargoes of interest in this pathway are a variety of lysosomal hydrolases, which are initially produced in the secretory pathway but then sorted to the endosome rather than being secreted outside the cell. Pharmacologic or genetic collapse of the *trans*-Golgi is known to impair this process and to result in defective lysosomal function(17).

Defects in *trans*-Golgi to late endosome transport can be evaluated by measuring the steady-state ratio of lysosomal hydrolases in the lysosome versus the secretory pathway; defective sorting results in decreased lysosomal enzyme content and increased secretory pathway content. We used density-dependent organelle fractionation of hypotonically-lysed cells to isolate the lysosomal (P2) and microsomal fractions (P3), and then performed immunoblotting for various proteins known to traffic to the lysosome. Three such proteins—LAMP1, GBA and ARSB—show decreased abundance in the lysosomal fraction and/or increased abundance in the microsomal fraction of cells deficient in LRRK2 and NSF compared to control cells (Fig. 6E). These data were reinforced with a quantitative enzymatic assay for N-acetylglucosaminidase (NAG) activity, which is mediated by the lysosomal enzyme hexosaminidase-B. Data from this

assay also showed increased NAG activity in the microsomal fraction and decreased activity in the lysosomal fraction of cells deficient in LRRK2 and NSF compared to control cells (Fig. 6F). Together these data imply that the undigested waste material seen in cellular vesicles by electron microscopy (Fig. 3B-D) accumulates due to insufficient trafficking of digestive hydrolases to the lysosome due to *trans*-Golgi fragmentation.

In contrast to the defects in endocytic recycling, we did not find any evidence of acute defects in autophagic flux in HK2 cells after knockdown of LRRK2 or NSF. Cells starved of amino acids to induce autophagy demonstrated proper accumulation and subsequent turnover of LC3B and p62/SQSTM1 protein over a 10 hour timecourse, suggesting that macroautophagy itself is not defective when LRRK2 or NSF is depleted from HK2 cells (Fig. 6G-J).

Discussion

The discovery of PD-associated mutations in the gene encoding LRRK2 in 2004 produced a surge of interest in how this protein works at the cellular level(30, 39). In the years since that discovery, a wealth of research has demonstrated that LRRK2 primarily functions as a regulator of vesicle trafficking in a variety of cell types including neurons, immune cells and in specific epithelial cell populations. Of these latter cell types, Type II pneumocytes of the lung and proximal renal tubule cells have received the most attention due to their especially high expression of LRRK2 and their pathophysiological deficits upon *Lrrk2* deletion in rodent models(4, 19). Prior studies of these animal models have demonstrated the progressive accumulation of undigested cellular contents within a poorly defined vesicular compartment that bears features of the late endosome, lysosome and autophagosome(37, 38).

Precisely how and why this population of vesicles accumulates in the renal epithelium has been of significant interest for three reasons. In the first place, identification of the molecular defects in these cells could potentially provide insights into the cellular pathophysiology of neurons in Parkinson's Disease, thereby providing new therapeutic targets for treatment. Secondly, identification of peripheral disease markers in patients bearing LRRK2 mutations could potentially provide a means for non-invasive monitoring of disease progression and response to therapy via urine sampling, which is far more tractable than cerebrospinal fluid or tissue sampling(13). Finally, the observation that genetic deletion of *Lrrk2* in mice leads to significant pathology in the lung and kidney suggested that prolonged systemic treatment of PD patients with pharmacologic inhibitors of LRRK2 enzymatic activity could be toxic to these organs, thus

obviating this approach as a therapy in PD. While the realization of this concern has varied among the various LRRK2 inhibitors developed to date, it remains a significant issue given that patients treated in such fashion could conceivably be dosed for decades due to the chronic and progressive nature of PD(10, 18).

In this study we developed a cellular model of LRRK2 deficiency in normal immortalized human kidney cells derived from the proximal tubule, which is primarily where LRRK2 is expressed in the kidney(23). These cells phenocopy the early renal defects seen in *Lrrk2-/-* mice, including the presence of an enlarged late endosomal compartment and accumulation of vesicles with undigested lysosomal cargo. Most importantly, we demonstrate that the LRRK2-NSF interaction is conserved in human kidney cells, and that loss of LRRK2 leads to a compensatory destabilization of NSF and Golgi fragmentation. Trafficking of cargo to and from the Golgi is consequently disrupted by loss of either LRRK2 or NSF, suggesting that the molecular interaction between these two proteins is critical for the maintenance of vesicular trafficking homeostasis in the kidney.

These findings provide important insights into the etiology of endo-lysosomal dysfunction in cells with deficiency or inhibition of LRRK2 by profiling the various vesicle trafficking defects in these cells. Though prior studies both *in vitro* and *in vivo* have noted the defects in Golgi organization associated with LRRK2 deficits, they did not functionally connect these defects to the accumulation of undigested waste vesicles that are also observed in these cells(21, 22). Here we show that the fragmentation of the entire Golgi apparatus in LRRK2 deficient cells leads to deficits in *trans*-Golgi to lysosome trafficking, including the trafficking of important lysosomal hydrolases. Collectively these data implicate defects in Golgi apparatus organization and structure as the primary cause for lysosomal dysfunction in renal cells lacking LRRK2.

In this context, it is worth noting that genes whose absence or mutation cause similar defects in protein trafficking have previously been associated with PD, including the genes encoding glucocerebrosidase (GBA) and the retromer complex component VPS35(9, 25). Whether this implies a general mechanism for the onset of cellular toxicity in PD is unclear at this time, particularly since the relationship of lysosomal dysfunction to the other cardinal hallmarks of PD—mitochondrial dysfunction and alpha-synuclein aggregation—remains somewhat obscure(9). Given the growing number of vesicle trafficking proteins that have been connected

to this disease, however, the ongoing search for a unifying mechanism is of considerable importance.

One final point of interest regarding LRRK2 and human disease should be noted in the context of renal cancer. Both we and others have implicated LRRK2 amplification and hyperactivity in the Type I subset of papillary renal cell carcinomas that account for about 10% of all human kidney cancer(2, 23). We speculate that these tumors, which are driven by aberrant receptor tyrosine kinase signaling through the hepatocyte growth factor (HGF) receptor MET, may select for LRRK2 amplification (chromosome 12q12) to promote mistrafficking of MET away from lysosomes and toward the endosome-to-Golgi recycling pathway. Given that LRRK2 knockdown seems to enhance the rate of trafficking from endosomes to the lysosome, it is possible that the converse event—hyperactivation of LRRK2 activity—would slow trafficking of endocytic cargo to the lysosome, leading to aberrant stabilization of MET. We intend to address this question in future studies as a means of providing insights into the molecular events leading to cellular transformation in the human kidney.

Acknowledgements

We would like to thank Dr. Ted Dawson (Johns Hopkins) for his provision of fixed embedded renal tissue from *Lrrk2* knockout mice, and Dr. Jaclyn Henderson (Pfizer, New York, NY) for provision of the LRRK2 inhibitor PFE-06447475.

This work has been supported by the National Institutes of Health with funding from grant number 1-R15-CA192094 (National Cancer Institute). No competing interests or disclosures are declared by any author involved in this work.

Author current addresses:

Nathan J. Lanning
California State University, Department of Biology, 5151 State University Drive, Los Angeles, CA 90032 USA

Calvin VanOpstall
University of Chicago, Ben May Department for Cancer Research, 5841 South Maryland Ave, Chicago, Illinois 60637

Megan L. Goodall
University of Colorado Denver, Department of Pharmacology, 12801 East 17th Ave, Aurora CO 80045

Jeffrey P. MacKeigan
Michigan State University College of Human Medicine, Department of Obstetrics, Gynecology & Reproductive Biology, 15 Michigan St. NE, Grand Rapids, MI 49503

References

1. **Agalliu I, San Luciano M, Mirelman A, Giladi N, Waro B, Aasly J, Inzelberg R, Hassin-Baer S, Friedman E, Ruiz-Martinez J, Marti-Masso JF, Orr-Urtreger A, Bressman S, and Saunders-Pullman R**. Higher frequency of certain cancers in LRRK2 G2019S mutation carriers with Parkinson disease: a pooled analysis. *JAMA neurology* 72: 58-65, 2015.

2. **Albiges L, Guegan J, Le Formal A, Verkarre V, Rioux-Leclercq N, Sibony M, Bernhard JC, Camparo P, Merabet Z, Molinie V, Allory Y, Orear C, Couve S, Gad S, Patard JJ, and Escudier B**. MET is a potential target across all papillary renal cell carcinomas: result from a large molecular study of pRCC with CGH array and matching gene expression array. *Clinical cancer research : an official journal of the American Association for Cancer Research* 20: 3411-3421, 2014.

3. **Alegre-Abarrategui J, Christian H, Lufino MM, Mutihac R, Venda LL, Ansorge O, and Wade-Martins R**. LRRK2 regulates autophagic activity and localizes to specific membrane microdomains in a novel human genomic reporter cellular model. *Human molecular genetics* 18: 4022-4034, 2009.

4. **Baptista MA, Dave KD, Frasier MA, Sherer TB, Greeley M, Beck MJ, Varsho JS, Parker GA, Moore C, Churchill MJ, Meshul CK, and Fiske BK**. Loss of leucine-rich repeat kinase 2 (LRRK2) in rats leads to progressive abnormal phenotypes in peripheral organs. *PloS one* 8: e80705, 2013.

5. **Beckers CJ, Block MR, Glick BS, Rothman JE, and Balch WE**. Vesicular transport between the endoplasmic reticulum and the Golgi stack requires the NEM-sensitive fusion protein. *Nature* 339: 397-398, 1989.

6. **Beilina A, Rudenko IN, Kaganovich A, Civiero L, Chau H, Kalia SK, Kalia LV, Lobbestael E, Chia R, Ndukwe K, Ding J, Nalls MA, International Parkinson's Disease Genomics C, North American Brain Expression C, Olszewski M, Hauser DN, Kumaran R, Lozano AM, Baekelandt V, Greene LE, Taymans JM, Greggio E, and Cookson MR**. Unbiased screen for interactors of leucine-rich repeat kinase 2 supports a common pathway for sporadic and familial Parkinson disease. *Proceedings of the National Academy of Sciences of the United States of America* 111: 2626-2631, 2014.

7. **Belluzzi E, Gonnelli A, Cirnaru MD, Marte A, Plotegher N, Russo I, Civiero L, Cogo S, Carrion MP, Franchin C, Arrigoni G, Beltramini M, Bubacco L, Onofri F, Piccoli G, and Greggio E**. LRRK2 phosphorylates pre-synaptic N-ethylmaleimide sensitive fusion (NSF) protein enhancing its ATPase activity and SNARE complex disassembling rate. *Molecular neurodegeneration* 11: 1, 2016.

8. **Block MR, Glick BS, Wilcox CA, Wieland FT, and Rothman JE**. Purification of an N-ethylmaleimide-sensitive protein catalyzing vesicular transport. *Proceedings of the National Academy of Sciences of the United States of America* 85: 7852-7856, 1988.

9. **Dehay B, Martinez-Vicente M, Caldwell GA, Caldwell KA, Yue Z, Cookson MR, Klein C, Vila M, and Bezard E**. Lysosomal impairment in Parkinson's disease. *Movement disorders : official journal of the Movement Disorder Society* 28: 725-732, 2013.

10. **Estrada AA, Liu X, Baker-Glenn C, Beresford A, Burdick DJ, Chambers M, Chan BK, Chen H, Ding X, DiPasquale AG, Dominguez SL, Dotson J, Drummond J, Flagella M, Flynn S, Fuji R, Gill A, Gunzner-Toste J, Harris SF, Heffron TP, Kleinheinz T, Lee DW, Le Pichon CE, Lyssikatos JP, Medhurst AD, Moffat JG, Mukund S, Nash K, Scearce-Levie K, Sheng Z, Shore DG, Tran T, Trivedi N, Wang S, Zhang S, Zhang X, Zhao G, Zhu H, and Sweeney ZK**. Discovery of highly potent, selective, and brain-penetrable leucine-rich repeat kinase 2 (LRRK2) small molecule inhibitors. *Journal of medicinal chemistry* 55: 9416-9433, 2012.

11. **Fan J, Zhou X, Wang Y, Kuang C, Sun Y, Liu X, Toomre D, and Xu Y**. Differential requirement for N-ethylmaleimide-sensitive factor in endosomal trafficking of transferrin receptor from anterograde trafficking of vesicular stomatitis virus glycoprotein G. *FEBS Lett* 591: 273-281, 2017.

12. **Forbes SA, Beare D, Bindal N, Bamford S, Ward S, Cole CG, Jia M, Kok C, Boutselakis H, De T, Sondka Z, Ponting L, Stefancsik R, Harsha B, Tate J, Dawson E, Thompson S, Jubb H, and Campbell PJ**. COSMIC: High-Resolution Cancer Genetics Using the Catalogue of Somatic Mutations in Cancer. *Current protocols in human genetics* 91: 10 11 11-10 11 37, 2016.

13. **Fraser KB, Moehle MS, Daher JP, Webber PJ, Williams JY, Stewart CA, Yacoubian TA, Cowell RM, Dokland T, Ye T, Chen D, Siegal GP, Galemmo RA, Tsika E, Moore DJ, Standaert DG, Kojima K, Mobley JA, and West AB**. LRRK2 secretion in exosomes is regulated by 14-3-3. *Human molecular genetics* 22: 4988-5000, 2013.

14. **Fuji RN, Flagella M, Baca M, Baptista MA, Brodbeck J, Chan BK, Fiske BK, Honigberg L, Jubb AM, Katavolos P, Lee DW, Lewin-Koh SC, Lin T, Liu X, Liu S, Lyssikatos JP, O'Mahony J, Reichelt M, Roose-Girma M, Sheng Z, Sherer T, Smith A, Solon M, Sweeney ZK, Tarrant J, Urkowitz A, Warming S, Yaylaoglu M, Zhang S, Zhu H, Estrada AA, and Watts RJ**. Effect of selective LRRK2 kinase inhibition on nonhuman primate lung. *Science translational medicine* 7: 273ra215, 2015.

15. **Goldenring JR**. A central role for vesicle trafficking in epithelial neoplasia: intracellular highways to carcinogenesis. *Nature reviews Cancer* 13: 813-820, 2013.

16. **Greggio E, Jain S, Kingsbury A, Bandopadhyay R, Lewis P, Kaganovich A, van der Brug MP, Beilina A, Blackinton J, Thomas KJ, Ahmad R, Miller DW, Kesavapany S, Singleton A, Lees A, Harvey RJ, Harvey K, and Cookson MR**. Kinase activity is required for the toxic effects of mutant LRRK2/dardarin. *Neurobiology of disease* 23: 329-341, 2006.

17. **Gu F, Crump CM, and Thomas G**. Trans-Golgi network sorting. *Cell Mol Life Sci* 58: 1067-1084, 2001.

18. **Henderson JL, Kormos BL, Hayward MM, Coffman KJ, Jasti J, Kurumbail RG, Wager TT, Verhoest PR, Noell GS, Chen Y, Needle E, Berger Z, Steyn SJ, Houle C, Hirst WD, and Galatsis P**. Discovery and preclinical profiling of 3-[4-(morpholin-4-yl)-7H-pyrrolo[2,3-d]pyrimidin-5-yl]benzonitrile (PF-06447475), a highly potent, selective, brain penetrant, and in vivo active LRRK2 kinase inhibitor. *Journal of medicinal chemistry* 58: 419-432, 2015.

19. **Herzig MC, Kolly C, Persohn E, Theil D, Schweizer T, Hafner T, Stemmelen C, Troxler TJ, Schmid P, Danner S, Schnell CR, Mueller M, Kinzel B, Grevot A,**

Bolognani F, Stirn M, Kuhn RR, Kaupmann K, van der Putten PH, Rovelli G, and Shimshek DR. LRRK2 protein levels are determined by kinase function and are crucial for kidney and lung homeostasis in mice. *Human molecular genetics* 20: 4209-4223, 2011.

20. **Inzelberg R, Cohen OS, Aharon-Peretz J, Schlesinger I, Gershoni-Baruch R, Djaldetti R, Nitsan Z, Ephraty L, Tunkel O, Kozlova E, Inzelberg L, Kaplan N, Fixler Mehr T, Mory A, Dagan E, Schechtman E, Friedman E, and Hassin-Baer S**. The LRRK2 G2019S mutation is associated with Parkinson disease and concomitant non-skin cancers. *Neurology* 78: 781-786, 2012.

21. **Lin CH, Li H, Lee YN, Cheng YJ, Wu RM, and Chien CT**. Lrrk regulates the dynamic profile of dendritic Golgi outposts through the golgin Lava lamp. *J Cell Biol* 210: 471-483, 2015.

22. **Lin X, Parisiadou L, Gu XL, Wang L, Shim H, Sun L, Xie C, Long CX, Yang WJ, Ding J, Chen ZZ, Gallant PE, Tao-Cheng JH, Rudow G, Troncoso JC, Liu Z, Li Z, and Cai H**. Leucine-rich repeat kinase 2 regulates the progression of neuropathology induced by Parkinson's-disease-related mutant alpha-synuclein. *Neuron* 64: 807-827, 2009.

23. **Looyenga BD, Furge KA, Dykema KJ, Koeman J, Swiatek PJ, Giordano TJ, West AB, Resau JH, Teh BT, and MacKeigan JP**. Chromosomal amplification of leucine-rich repeat kinase-2 (LRRK2) is required for oncogenic MET signaling in papillary renal and thyroid carcinomas. *Proc Natl Acad Sci U S A* 108: 1439-1444, 2011.

24. **MacLeod DA, Rhinn H, Kuwahara T, Zolin A, Di Paolo G, McCabe BD, Marder KS, Honig LS, Clark LN, Small SA, and Abeliovich A**. RAB7L1 interacts with LRRK2 to modify intraneuronal protein sorting and Parkinson's disease risk. *Neuron* 77: 425-439, 2013.

25. **Mazzulli JR, Xu YH, Sun Y, Knight AL, McLean PJ, Caldwell GA, Sidransky E, Grabowski GA, and Krainc D**. Gaucher disease glucocerebrosidase and alpha-synuclein form a bidirectional pathogenic loop in synucleinopathies. *Cell* 146: 37-52, 2011.

26. **Migheli R, Del Giudice MG, Spissu Y, Sanna G, Xiong Y, Dawson TM, Dawson VL, Galioto M, Rocchitta G, Biosa A, Serra PA, Carri MT, Crosio C, and Iaccarino C**. LRRK2 affects vesicle trafficking, neurotransmitter extracellular level and membrane receptor localization. *PloS one* 8: e77198, 2013.

27. **Morgan A, Dimaline R, and Burgoyne RD**. The ATPase activity of N-ethylmaleimide-sensitive fusion protein (NSF) is regulated by soluble NSF attachment proteins. *J Biol Chem* 269: 29347-29350, 1994.

28. **Muller JM, Rabouille C, Newman R, Shorter J, Freemont P, Schiavo G, Warren G, and Shima DT**. An NSF function distinct from ATPase-dependent SNARE disassembly is essential for Golgi membrane fusion. *Nature cell biology* 1: 335-340, 1999.

29. **Mullock BM, Smith CW, Ihrke G, Bright NA, Lindsay M, Parkinson EJ, Brooks DA, Parton RG, James DE, Luzio JP, and Piper RC**. Syntaxin 7 is localized to late endosome compartments, associates with Vamp 8, and Is required for late endosome-lysosome fusion. *Mol Biol Cell* 11: 3137-3153, 2000.

30. **Paisan-Ruiz C, Jain S, Evans EW, Gilks WP, Simon J, van der Brug M, Lopez de Munain A, Aparicio S, Gil AM, Khan N, Johnson J, Martinez JR, Nicholl D, Carrera IM, Pena AS, de Silva R, Lees A, Marti-Masso JF, Perez-Tur J, Wood NW, and Singleton AB**. Cloning of the gene containing mutations that cause PARK8-linked Parkinson's disease. *Neuron* 44: 595-600, 2004.

31. **Piccoli G, Condliffe SB, Bauer M, Giesert F, Boldt K, De Astis S, Meixner A, Sarioglu H, Vogt-Weisenhorn DM, Wurst W, Gloeckner CJ, Matteoli M, Sala C, and Ueffing M**. LRRK2 controls synaptic vesicle storage and mobilization within the recycling pool. *The Journal of neuroscience : the official journal of the Society for Neuroscience* 31: 2225-2237, 2011.

32. **Rabouille C, Kondo H, Newman R, Hui N, Freemont P, and Warren G**. Syntaxin 5 is a common component of the NSF- and p97-mediated reassembly pathways of Golgi cisternae from mitotic Golgi fragments in vitro. *Cell* 92: 603-610, 1998.

33. **Saunders-Pullman R, Barrett MJ, Stanley KM, Luciano MS, Shanker V, Severt L, Hunt A, Raymond D, Ozelius LJ, and Bressman SB**. LRRK2 G2019S mutations are associated with an increased cancer risk in Parkinson disease. *Movement disorders : official journal of the Movement Disorder Society* 25: 2536-2541, 2010.

34. **Sheng Z, Zhang S, Bustos D, Kleinheinz T, Le Pichon CE, Dominguez SL, Solanoy HO, Drummond J, Zhang X, Ding X, Cai F, Song Q, Li X, Yue Z, van der Brug MP, Burdick DJ, Gunzner-Toste J, Chen H, Liu X, Estrada AA, Sweeney ZK, Scearce-Levie K, Moffat JG, Kirkpatrick DS, and Zhu H**. Ser1292 autophosphorylation is an indicator of LRRK2 kinase activity and contributes to the cellular effects of PD mutations. *Science translational medicine* 4: 164ra161, 2012.

35. **Shin N, Jeong H, Kwon J, Heo HY, Kwon JJ, Yun HJ, Kim CH, Han BS, Tong Y, Shen J, Hatano T, Hattori N, Kim KS, Chang S, and Seol W**. LRRK2 regulates synaptic vesicle endocytosis. *Experimental cell research* 314: 2055-2065, 2008.

36. **Steger M, Tonelli F, Ito G, Davies P, Trost M, Vetter M, Wachter S, Lorentzen E, Duddy G, Wilson S, Baptista MA, Fiske BK, Fell MJ, Morrow JA, Reith AD, Alessi DR, and Mann M**. Phosphoproteomics reveals that Parkinson's disease kinase LRRK2 regulates a subset of Rab GTPases. *eLife* 5: 2016.

37. **Tong Y, Giaime E, Yamaguchi H, Ichimura T, Liu Y, Si H, Cai H, Bonventre JV, and Shen J**. Loss of leucine-rich repeat kinase 2 causes age-dependent bi-phasic alterations of the autophagy pathway. *Molecular neurodegeneration* 7: 2, 2012.

38. **Tong Y, Yamaguchi H, Giaime E, Boyle S, Kopan R, Kelleher RJ, 3rd, and Shen J**. Loss of leucine-rich repeat kinase 2 causes impairment of protein degradation pathways, accumulation of alpha-synuclein, and apoptotic cell death in aged mice. *Proceedings of the National Academy of Sciences of the United States of America* 107: 9879-9884, 2010.

39. **Zimprich A, Biskup S, Leitner P, Lichtner P, Farrer M, Lincoln S, Kachergus J, Hulihan M, Uitti RJ, Calne DB, Stoessl AJ, Pfeiffer RF, Patenge N, Carbajal IC, Vieregge P, Asmus F, Muller-Myhsok B, Dickson DW, Meitinger T, Strom TM, Wszolek ZK, and Gasser T**. Mutations in LRRK2 cause autosomal-dominant parkinsonism with pleomorphic pathology. *Neuron* 44: 601-607, 2004.

825

826

Figure Captions

Figure 1. LRRK2 deficiency disrupts vesicular trafficking in renal epithelia.

(A) H&E images of the renal cortex of wild-type (*Lrrk2*+/+) and knockout (*Lrrk2*-/-) mice at 3 months of age. (B) Brightfield images of normal human kidney (HK2) cells stably transduced with vectors expressing non-targeting (NT-sh) and LRRK2 shRNAs. Scale bar indicates 70 microns. (C) Diagram of endocytic trafficking pathways in the mammalian cell, with different protein markers characteristic of each cellular compartment indicated. TGN, trans-golgi network; MVB, multi-vesicular body. (D-G) Confocal fluorescent images of HK2 cells transduced with shRNA vectors and co-stained for specific markers of intracellular compartments. (D) Rab5 and EEA1 mark the early endosome, (E) LC3B and p62 mark autophagasomes, (F) Rab7 and LAMP1 mark the late endosome/MVB and lysosome, respectively. (G) STX6 and gm130 mark the TGN and golgi network, respectively. (H) Quantification of HK2 cells that display swollen, Rab7-positive compartments. (I) Quantification of gm130-positive Golgi apparatus area in stable HK2 cell lines. (J) Quantification of gm-130-positive Golgi apparatus area in stable HK2 cell lines after accounting for whether cells are positive or negative for swollen, Rab7-positive compartments. Error bars indicate standard deviation of triplicate or quadruplicate experimental replicates (*, $p<0.05$, **$p<0.005$).

Figure 2. Pharmacologic inhibition of LRRK2 kinase activity causes abnormal Golgi compartment enlargement.

(A,B) Wild-type HK2 cells were treated with the catalytic LRRK2 inhibitors GNE-7915 and PFE-475 for the indicated times to demonstrate prolonged inhibition of LRRK2 activity, as demonstrated by S935 autophosphorylation. Protein levels of NSF, Rab7 and β-actin levels are unchanged by LRRK2 enzymatic inhibition. (C) Representative immunofluorescent images of HK2 cells treated with LRRK2 inhibitors and then stained with antibodies for gm-130 (red) and STX6 (green) to demonstrate increase in Golgi area after LRRK2 inhibition. (D) Quantification of gm130-positive Golgi apparatus area in normal HK2 cells after 1 hour treatment with 5 nM nocodazole or DMSO vehicle. (E) Quantification of gm130-positive Golgi apparatus area in normal HK2 cells after 24 hour treatment with 2 μM concentration of the indicated LRRK2 inhibitor or DMSO vehicle. Error bars indicate standard deviation of triplicate or quadruplicate experimental replicates (*, $p<0.05$, **$p<0.005$).

Figure 3. Depletion of NSF phenocopies LRRK2 deficiency and results in the accumulation of vesicular waste cargo.

(A) Confocal immunofluorescent images of HK2 cells transduced with non-targeting shRNAs or shRNAs targeted to LRRK2 or NSF. Cells were stained with antibodies for endogenous EEA1 (red) and Rab7 (green) to indicate the early and late endosomal compartments, respectively. DAPI (blue) co-stain of nuclei is also shown in the merged image. (B-D) Transmission electron microscopy was performed on dissociated cell pellets of HK2 cells that were stably depleted of LRRK2 or NSF using lentiviral shRNAs. (B) Whole cell images of stable lines showing the accumulation of electron-dense vesicles in HK2 cells after depletion of LRRK2 or NSF. Cells also displayed large vacuolar inclusions in some instances (red arrows). (C) Vesicles in HK2 cells lacking LRRK2 display whole organelles encased in vesicles (black arrows), which suggest that some of these vesicles may be autophagic in origin. (D) Higher magnification images of LRRK2-deficient HK2 cells demonstrate the variety of waste cargo in vesicles, which includes: (i) membrane whorls, (ii) lipid droplets, and (iii-iv) electron dense aggregates of undetermined identity.

Figure 4. LRRK2 and NSF physically and functionally interact in renal epithelia.

(A) Confocal immunofluorescent images of HK2 cells after transfection with FLAG-LRRK2 expression vectors to enable visualization of LRRK2 (red) with endogenous NSF (green). The inset in the merged panel is a 2.5x magnification of the indicated cell in this image. (B) Quantification of immunofluorescent signal colocalization between total LRRK2 and the FLAG epitope found on exogenous LRRK2 (positive control), and between NSF and the FLAG epitope using Pearson's and Mander's correlation methods. Data represent mean signal overlap from 200 cells for each condition imaged by confocal microscopy. Error bars represent standard deviations of these measurements. (C) Immunoblot of NSF and LRRK2 after endogenous co-immunoprecipitation with anti-LRRK2 antibodies. Cell lysis buffer with and without 2 mM N-ethylmaleimide (NEM) was used to harvest protein lysates from cells. Input samples represent 10% of the protein input used for immunoprecipitations. (D) Relative expression of NSF at the mRNA and protein levels in control, LRRK2 or NSF knockdown cell lines. Expression was determined as the ratio of NSF to RPL13A mRNA (q-RT-PCR) or β-actin protein (immunoblot), and then normalized to expression in non-targeting control cells (NT-sh). Error bars indicate standard deviations of triplicate samples. (E) Lysates were harvested from parental HK2 cells (control) and cells stably transfected with V5-tagged human NSF (nV5-NSF) after each line was infected with the indicated lentiviral shRNA vectors. Representative immunoblots demonstrate

NSF and V5-tag expression levels relative to actin in cells after introduction of shRNAs. (F) Immunoblot analysis of lysates from HK2 cells after infection with BacMam/FLAG-LRRK2 at various multiplicities of infection (shown as percent by volume of viral suspension used). Increasing LRRK2 levels has no impact on total levels of NSF protein in cells. Tubulin was used as a loading control to indicate equal loading between samples.

Figure 5. Golgi fragmentation in LRRK2 or NSF-deficient HK2 cells occurs independent of proliferation.

(A) Epifluorescent images of EdU-labeled stable HK2 cell lines. Positivity for EdU integration into the cellular genome (green nuclei) is indicative of S-phase entry. Cells were co-stained with antibodies for endogenous gm130 (red) to mark the Golgi network in each cell. (B) Quantification of EdU-positive cells in each stable cell line. (C) Quantification of gm130-positive Golgi apparatus area in stable HK2 cell lines. (D) Quantification of gm-130-positive Golgi apparatus area in stable HK2 cell lines after a single 2 hour pulse of EdU followed by immediate fixation and staining. (E) Quantification of gm-130-positive Golgi apparatus area in stable HK2 cell lines after a single 2 hour pulse of EdU followed by 6 hour media chase prior to fixation and staining. The quantified data account for whether cells are positive (gray) or negative (black) for EdU labeling in both panels (D) and (E). Error bars indicate standard deviation of values for triplicate experiments in which a minimum of 200 cells were quantified (*, $p<0.05$, **$p<0.005$).

Figure 6. LRRK2 deficiency alters the balance of vesicular trafficking between the late endosome and downstream compartments.

(A) Immunoblot for LRRK2, NSF, STX7 and tubulin in lysates of stable HK2 lines transduced with shRNA vectors to the indicated genetic target (NT, non-targeting). (B) Timecourse of fluid-phase, bulk endocytosis in stable HK2 lines by measuring uptake of AlexaFluor-488 labeled dextran. (C) Timecourse of receptor-mediated endocytosis by measuring uptake of AlexaFluor-488 labeled transferrin. Continuous uptake of transferrin depends upon recycling of the transferrin receptor from endosomes thru the trans-golgi network to the plasma membrane. (* $p<0.05$ relative to NT control) (D) Quantification of endocytic trafficking to the lysosome as a function of BZiPAR peptide uptake and conversion by lysosomal peptidases in the indicated HK2 stable lines. The dynamin inhibitor dynasore (30 μM) was added 15 minutes prior to BZiPAR (50 μM). (* $p<0.05$) (E) Immunoblot of the lysosomal proteins LAMP1, GBA and ARSB isolated by differential centrifugation from the indicated HK2 stable lines. (P2, lysosomal pellet; P3, microsomal pellet). (F) Quantification of N-acetylglucosaminidase (NAG) activity in the

lysosomal and microsomal fractions of stable HK2 cell lines. Error bars indicate standard deviations of three replicates (*, $p<0.05$). (G-J) Immunoblot analysis of lysates from the indicated stable HK2 cell lines after a timecourse treatment of amino acid starvation in the presence or absence of bafilomycin A1 (BafA1, 50 nM). Autophagic flux was monitored by the decreases in the adaptor protein SQSTM1 (p62) and the turnover in LC3B generated by induction of macroautophagy. Individual panels shown the timecourse results for controls cells infected with lentivirus containing a non-targeting shRNA (G) or shRNAs targeting LRRK2 (H), NSF (I), or STX7 (J). Actin levels were included to indicate equal loading of each sample.

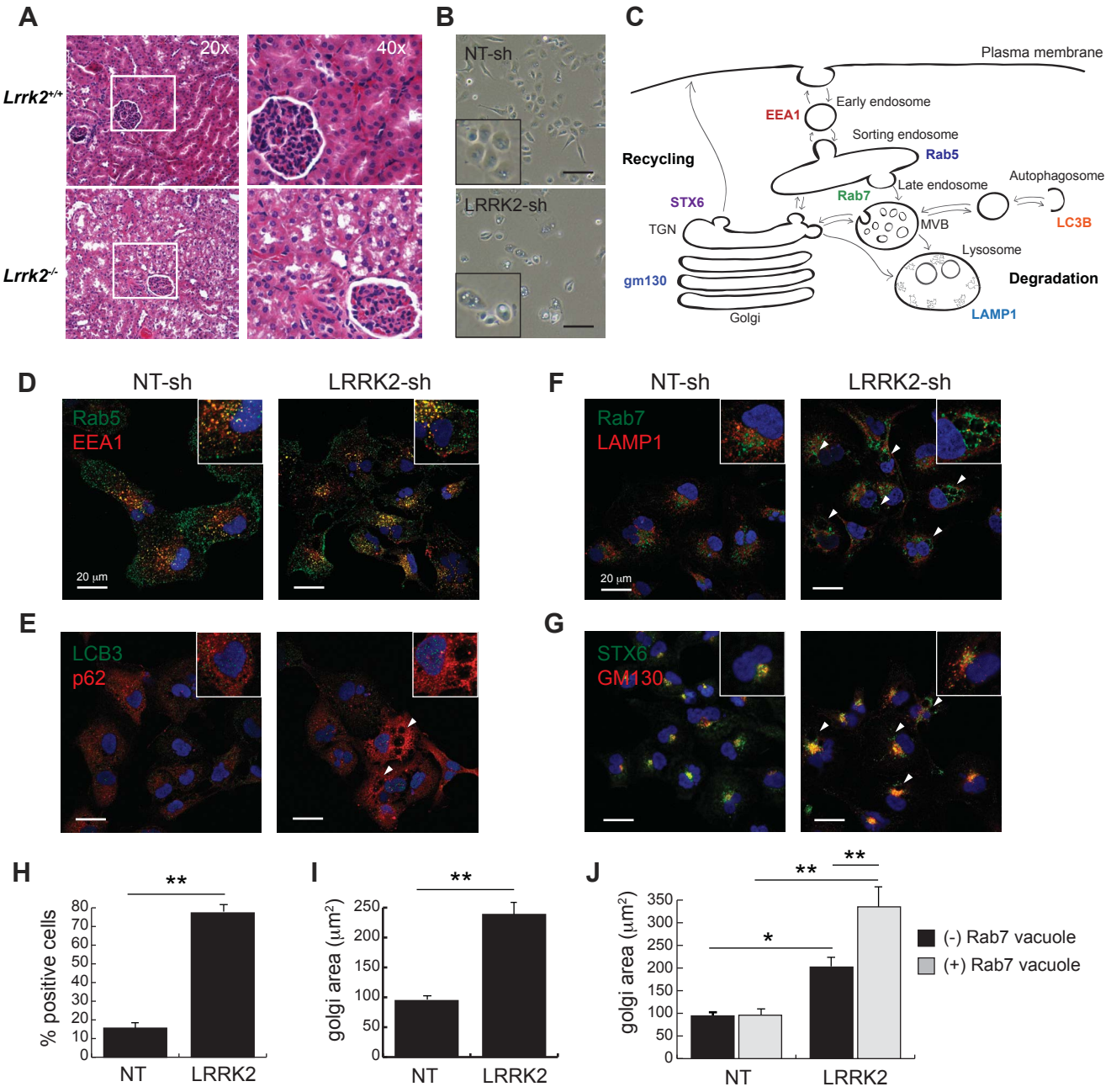

Figure 1

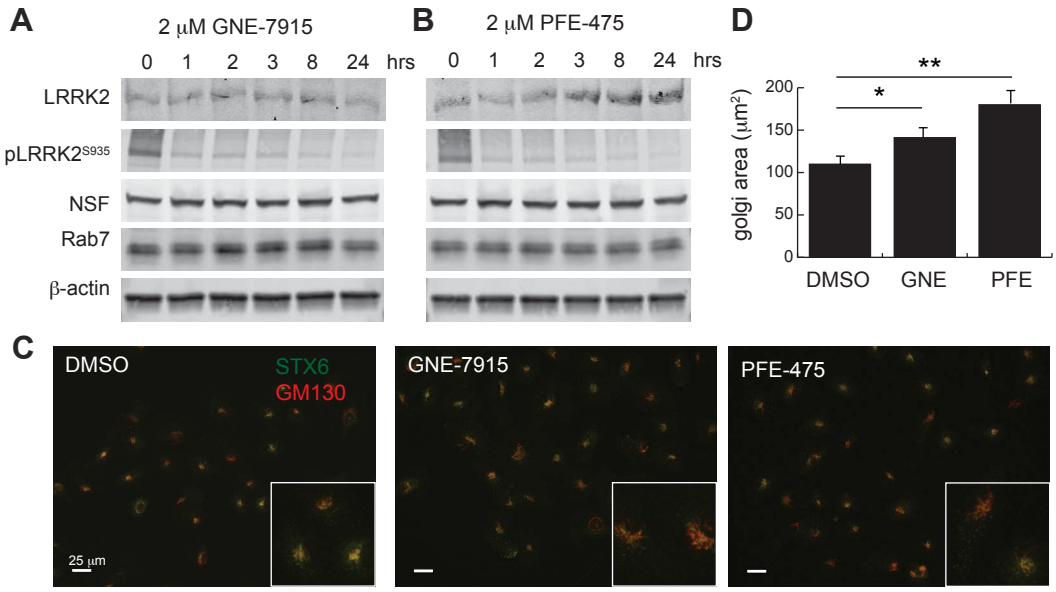

Figure 2

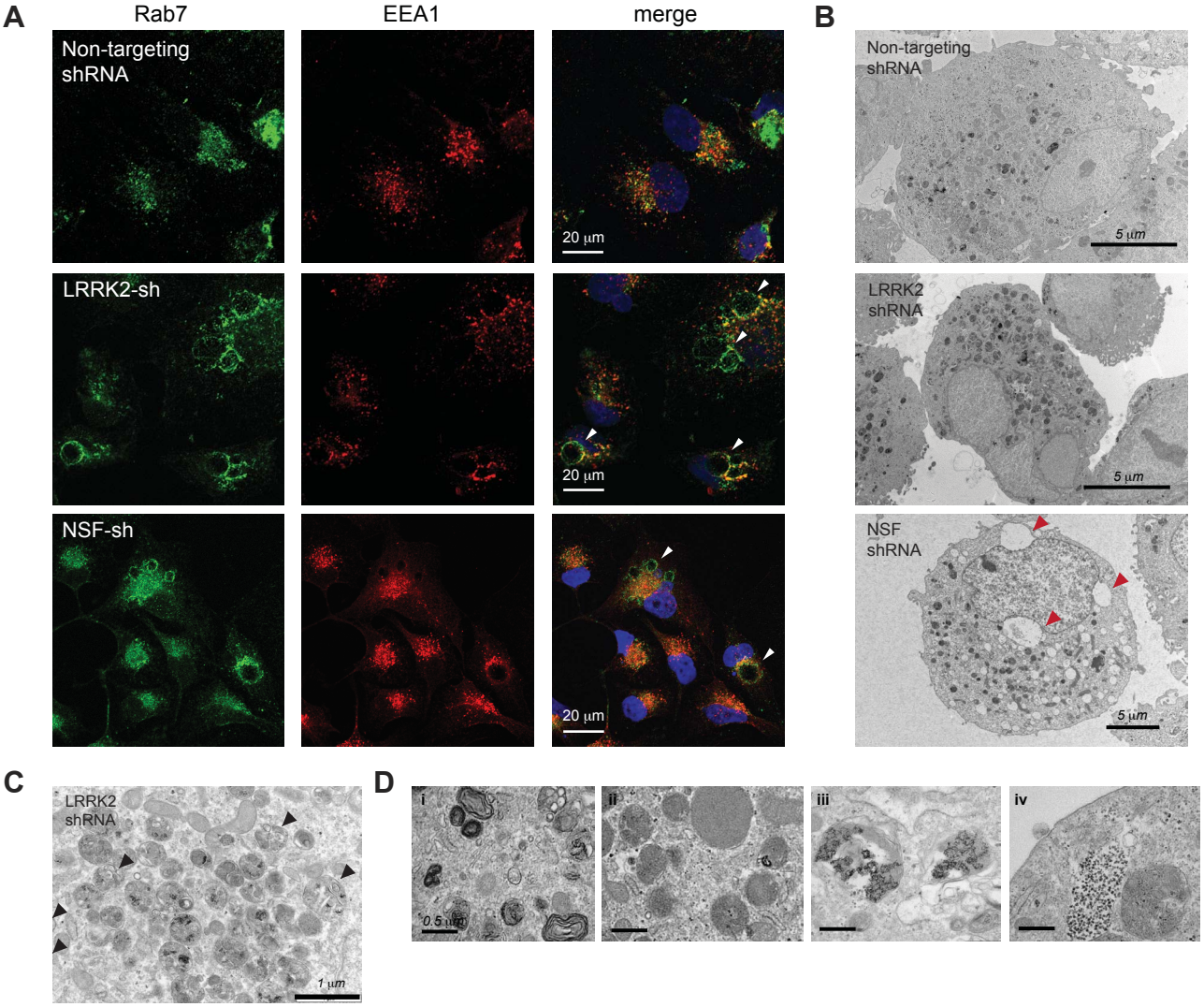

Figure 3

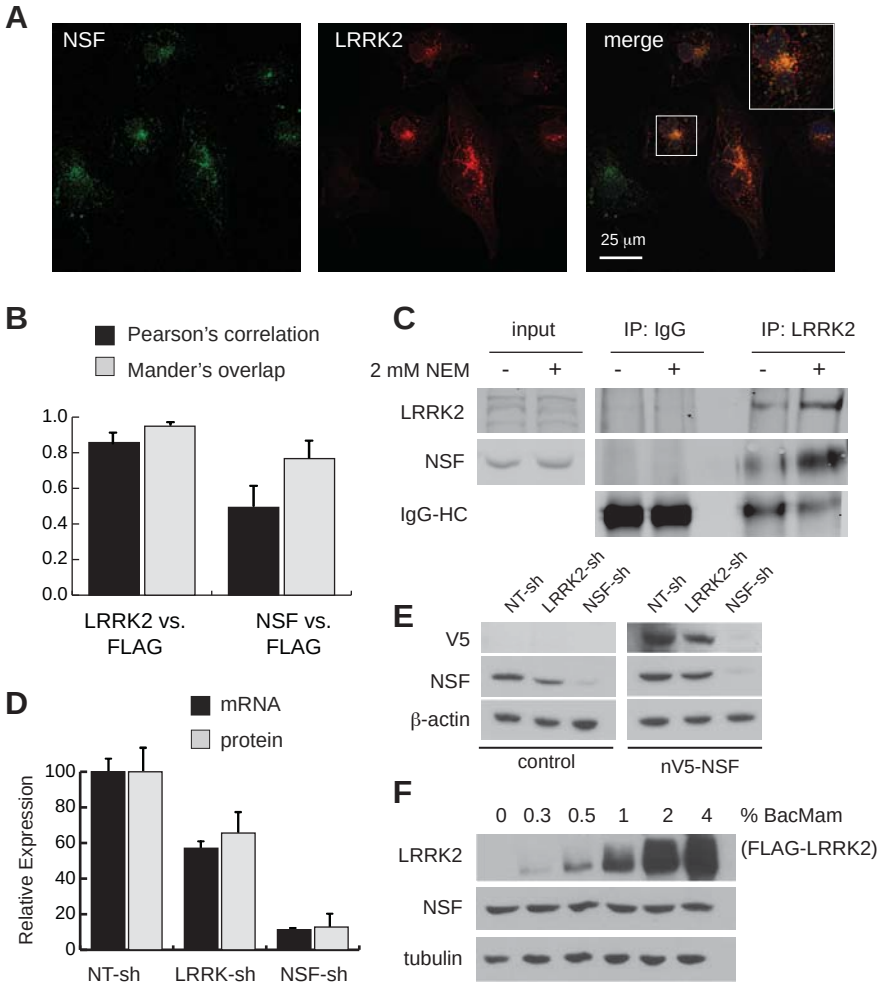

Figure 4

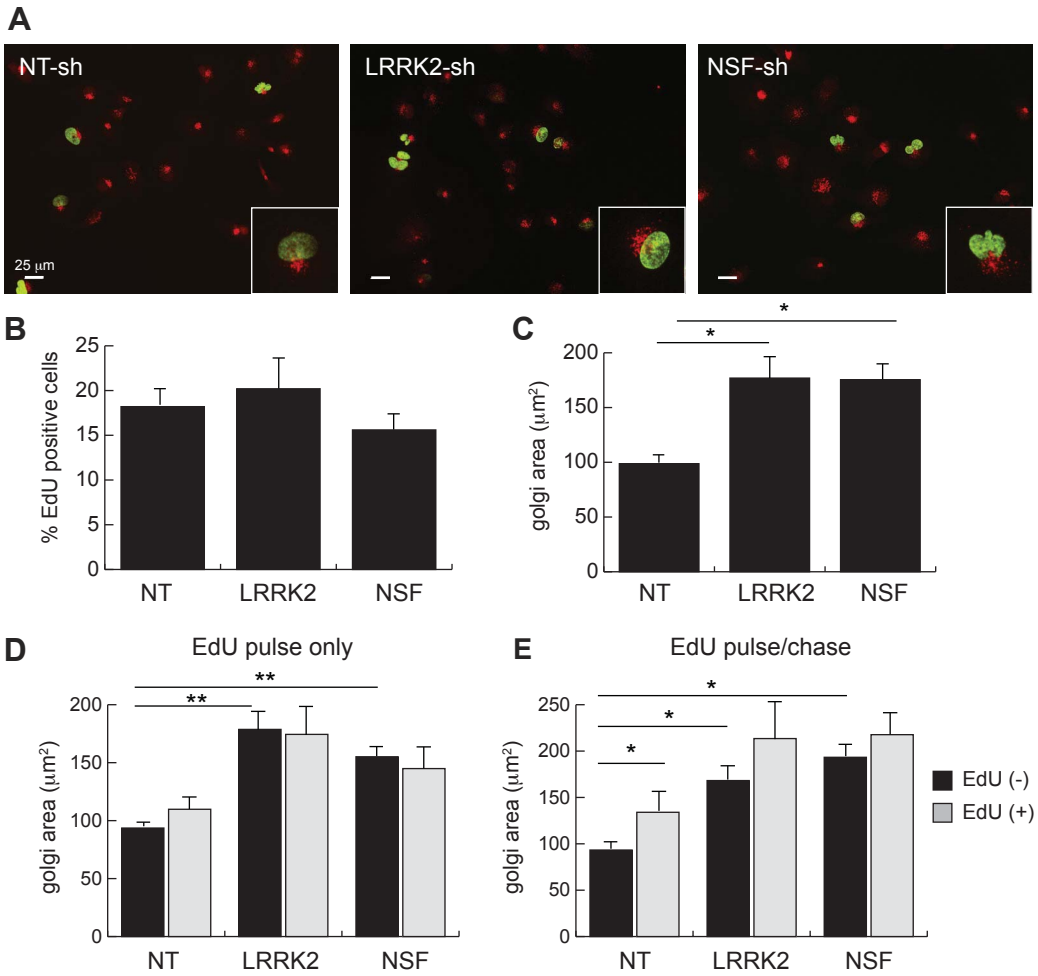

Figure 5

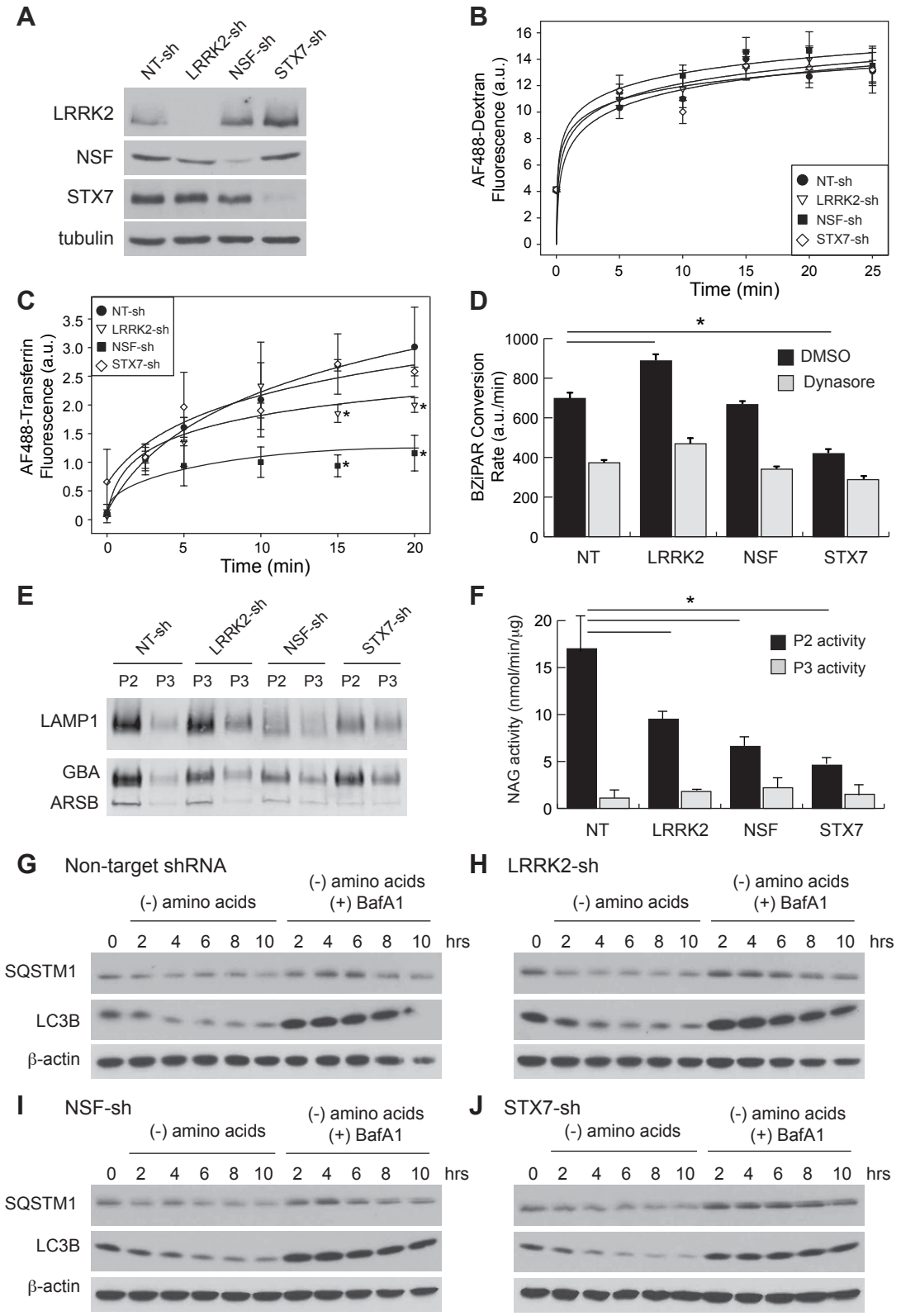

Figure 6